NASA TM X-54,024

SOME SOURCES OF GROUND-WIND LOADS IN LAUNCH VEHICLES

By Donald A. Buell
Research Scientist
NASA, Ames Research Center, Moffett Field, Calif.

Introduction

Prior to launch, a typical launch vehicle resembles a circular cylinder cantilevered from the base. One would like to be able to predict the loads which a wind will induce in such a structure. Air flow about circular cylinders has been studied extensively for subcritical Reynolds numbers, where the boundary layer is laminar up to the point of flow separation. Launch vehicles are often large enough that even a gentle breeze results in Reynolds numbers above this region. As a consequence, researchers are again studying the flow about cylinders, with emphasis on large Reynolds numbers. The task is difficult since boundary-layer transition is now a complicating factor. In addition, such factors as nose shape and protuberances which differentiate an actual vehicle from an ideal cylinder have proved to be important.

Investigation of the flow over simple cylinders has given needed insight into the flow behavior at supercritical Reynolds numbers. Fung[1] has described the forces on an essentially two-dimensional cylinder at Reynolds numbers near 1 million, in the lower portion of the supercritical region. He found that the force fluctuations on a segment of the cylinder were random in amplitude and frequency. Schmidt[2] used pressure measurements to establish that the fluctuating forces had little correlation between axial stations more than one or two diameters apart, in the same range of Reynolds numbers. Knowledge of the forcing frequencies and of the degree of correlation between the forces at various stations is required to predict the stresses in an elastic structure. Brief tests by Roshko[3] indicated the interesting possibility that the forces on a cylinder at Reynolds numbers above 5.5 million may be periodic.

Investigations of the problem have been conducted at Ames Research Center for some years in the range of Reynolds numbers from 1 to 10 million. However, the work has been confined to configurations approximating actual launch vehicles. Because interpretation of the results was often beclouded by unexpected trends, the work has developed into an exploratory type of investigation aimed at providing a better perspective of the effects of the many variables involved with such vehicles. The greatest part of the effort has been expended in establishing the lateral oscillatory loads since these are the least predictable of the various components. This paper is a summary of the major factors contributing to lateral oscillations of launch-vehicle models observed at Ames. Most of the results are previously unreported. A complete presentation of the available test results will not be attempted here; only those data necessary to illustrate the main points will be shown.

All of the results discussed herein were obtained in a steady wind having a very low turbulence level. As such, they cannot be considered strictly applicable to vehicles in a natural atmospheric environment. However, loads measured in a more natural environment cannot be generally applied, either, until all of the critical factors have been taken into account. Therefore, this paper is primarily a guide to further investigation.

Notation

$C_{l,d}$	lateral dynamic bending-moment coefficient, $\frac{(M_l)_{max}}{qAL}\sqrt{\frac{V}{fD}}\sqrt{\zeta}$ Mr
A	frontal area of model, sq ft
D	upper-stage diameter, ft
f	first cantilever mode frequency in lateral direction, cps
K	structural parameter, Mr
L	model length, ft
M	generalized mass, $\int_0^L \varphi^2 \, m \, dy$, slugs
M^1	base bending moment per unit tip deflection in first cantilever mode, lb
$(M_l)_{max}$	maximum value of lateral dynamic base bending moment in first cantilever mode for 1-minute data sample, ft-lb
m	mass per unit length, slugs/ft
N	number related to structural characteristics of the model, $\frac{M}{M^1}(2\pi f)^2 L$
q	free-stream dynamic pressure, $\frac{1}{2}\rho V^2$, psf
R	Reynolds number, $\frac{\rho V D}{\mu}$
r	"generalized" fineness ratio, $\frac{1}{\int_0^1 \varphi \frac{x}{L} d\left(\frac{y}{L}\right)}$
V	free-stream velocity, fps
x	local diameter, ft
y	axial distance from base to model station, ft
ζ	ratio of lateral structural damping in first cantilever mode to critical damping
μ	air viscosity, slugs per foot second

ρ air density, slugs per cubic foot

φ mode shape of first cantilever mode, $\frac{\text{local deflection}}{\text{tip deflection}}$

Tests and Data Reduction

The models discussed herein are sketched in Fig. 1. The models were built of aluminum or steel with internal weights such that the first cantilever bending characteristics of hypothetical vehicles were simulated. The configurations evolved from tests with contractors who were simulating real vehicles, but modifications have been made to the configurations for research purposes. Consequently, the models do not represent any actual vehicle. The models were bolted directly to the floor structure of the Ames 12-foot pressure tunnel, and bending moments were measured by means of strain gages inside the model. Circular horizontal plates were placed under the noses of models A and C for some of the tests and are indicated on the sketches with dashed lines. Model B and the associated instrumentation have been previously described.[4]

External conduits were simulated by rods attached to the model as shown in Fig. 2. An umbilical tower with a solid blast shield next to the vehicle was simulated by a box structure, shown in Fig. 3. The screen on the front and sides represents pipes and conduits that fill an actual tower. The tower was symmetrical with respect to a plane through the model and tower axes.

A sample of the bending moments measured at the base of model A without conduits or tower is presented in Fig. 4. Both average and oscillatory components are shown as a function of test velocity. Each point on the curves of oscillatory moments is the maximum measured in about 1,300 cycles of oscillation in the first cantilever mode. The Reynolds numbers noted on this and other figures are based on the upper stage diameter. Large Reynolds numbers were obtained by testing at velocities up to three-tenths of the speed of sound with air density in the wind tunnel about five times normal atmospheric density.

One purpose of Fig. 4 is to show the size of the loads induced in a model with relatively little tendency to oscillate. The structural damping of the model (about 0.4 percent of critical) was less than that of a typical full-scale vehicle; hence, the oscillatory loads are higher than would be realized with the proper damping. Nevertheless, lateral oscillatory loads at least half the size of the average dragwise loads would be expected for this configuration. This relation provides a basis for evaluating the significance of the factors which increase the oscillations.

To facilitate comparisons, the lateral oscillatory loads were converted to response coefficients, as shown in Fig. 5. The coefficient ..... involves structural factors and is designed to be independent of model characteristics on the assumptions that the excitation is random and independent of the response. Reference 4 discusses the formulation of the coefficient. The test velocity was converted to reduced velocity, V/fD, following the practice of earlier investigators. For the case shown, which is to be the basis of comparison, the response coefficient is constant at approximately 2 over a wide range of velocities.

Results

Conduit Effects

A conduit on the stagnation line increased the oscillation by an order of magnitude, as shown in Fig. 6. Data are shown for conduits with diameters 1/16 and 1/32 of the upper stage diameter. Both sizes were tried on the upper stage, and the larger size, on the lower stage only. The fairing of the data is extended beyond the data points in cases where the oscillations were increasing rapidly and emergency stops were necessary. It was observed that the model motion had a much more nearly constant amplitude at the very large coefficients than at the smaller ones. This seemed to indicate a definite departure from the random response associated with supercritical Reynolds numbers. Less effect was produced as the conduits were reduced in size or were located lower on the model.

Model A was also tested with a horizontal plate under the nose. The purpose of the plate was to eliminate the effect of the nose on the flow around the cylindrical sections. The data are shown in Fig. 7 for two model dampings and two conduit shapes. Looking first at the results for the basic configuration, one can see that there were large responses at low speeds, as before. (It was possible to extend the data to high speeds by passing rapidly through the first region of large response.) By comparison with Fig. 6, it appears that the only effect of the plate was to move the conduit effects to slightly higher speeds. A more significant change in response was caused by increasing the damping. This result together with observations of a large constant-amplitude motion lead to the deduction that motion of the model caused much of the existing excitation. It would appear that an accurate simulation of a vehicle with conduits requires the duplication of factors, such as damping and relative density ratio, which affect the motion of the vehicle when subjected to a transient excitation. The conduit effect was entirely eliminated by fairing the conduit with tape.

The addition of other conduits in certain positions also eliminated the excitation caused by the upstream conduit. Figure 8 shows the response of the model with two conduits in various positions. When the second conduit was 180° from the stagnation line, the response was large, but when the second conduit was placed at 90°, it seemed to fix the point of separation so that the upstream disturbance was cancelled. Results not shown here indicate that a faired conduit at 90° could not reduce the response as effectively as the unfaired conduit did. Models with three or four conduits of equal size tended to produce less oscillation than models with one conduit larger than the others.

One other conduit position is worthy of comment. Figure 9 presents data for the 135° position. It was impossible to obtain consistent results in separate sweeps through the speed range with this conduit arrangement. Nevertheless, the condition occasionally produced some rather large responses.

It may be noted that the conduit increased the response at about the same speed whether it was mounted on the upper stage or the lower stage. This and other data tended to indicate that the adverse conduit effects were related to the Reynolds number of the conduit, rather than the Reynolds number or reduced velocity parameter for the cylinder.

Tower Effects

Another source of large oscillation was an umbilical tower. The one considered here was somewhat unusual in location and shape and is not intended to represent a typical tower. The critical wind orientation was with the model directly downwind from the tower. Figure 10 shows response coefficients for two spacings between the tower and model. The tower evidently acted as a flat plate and periodically shed vortices onto the model. Some idea of the wake pattern is given by the fact that the average dragwise moments on the model were negative in both situations shown. Other tests indicated that changes in model appendages or damping or frequency would not materially change the coefficients.

A number of tower fixes were tested, including removal of material from the solid face. The most effective modification was a solid plate which was attached to either the upstream or downstream face of the tower and projected on both sides. The wider the plate was, the more effective it was. A plate twice the width of the tower and covering only the area in front of the upper stage reduced the maximum response by a factor of 3, for the closer tower location.

Nose Effects

It has been established by a number of investigators that the nose of a vehicle is a source of excitation. A research shape that is particularly conducive to induced oscillations is a hemisphere. Figure 11 shows a photograph of oil on the surface of model B, which has such a nose. The line of flow separation is outlined by the accumulation of oil along the irregular line at the right of the picture. The separation line terminates below the tip of the model, and air appears to flow over the top and down into the wake behind the cylindrical part of the model. Data[4] have been published showing that this nose shape affects the pressure fluctuations on the cylindrical sections for at least 2 diameters below the nose. The effect of the nose can be easily nullified with a tip spoiler, which prevents the flow of air down into the wake of the upper stage.

Typical coefficients for a hemisphere-nose configuration are shown in Fig. 12. The response induced by a blunt nose was found to be sensitive to the roughness of the cylindrical sections near the nose. Strips of tape 0.003 inch thick were used to simulate the roughness on this model, although grit has produced the same effects. The response with roughness tended to be more sensitive to changes in reduced velocity than to changes in Reynolds number. It was concluded that the roughness promoted an early and straight transition of the boundary layer. The added roughness did not increase the pressure fluctuations, however, except near the nose. No coupling of the model motion and the excitation was apparent. A variety of nose shapes approximating the hemisphere have been observed to induce similar response characteristics.

One way of creating separation on the nose and thus reducing the adverse nose effects is to stretch the nose longitudinally into shapes with high fineness ratios. The beneficial effects of changing to such nose shapes have been reported,[4] but a few important exceptions were noted. Tests of model C have also demonstrated the possibility of large excitation under certain conditions. This model has a nose with a 29° included angle. Since the model has a constant diameter up to the nose, the area potentially under the influence of the nose is large. Figure 13 presents data for the model with and without a plate under the nose. The large reduction in response caused by the plate indicates that the flow around the nose was responsible for the excitation. In addition, the characteristics that indicate a coupling between model motion and excitation were observed. That is, the amplitude became constant, and an increase in damping reduced the coefficients. It was also noted that protuberances on the model generally reduced the tendency for oscillation. The large response shown in Fig. 13 is therefore the result of a rather special combination of factors. From observations of other models it is believed that noses with small cone angles may also induce oscillations, but the effect will occur at higher speeds than for blunt cones.

Concluding Remarks

In summary, test results obtained on models in a steady wind have been presented to indicate potential sources of oscillations induced by ground winds in launch vehicles. The following caused large oscillations:

1. single conduits
2. an umbilical tower
3. blunt noses

It was indicated that model motion and roughness accentuate the wind excitation in certain cases.

References

1. Fung, Y. C.: Fluctuating Lift and Drag Acting on a Cylinder in a Flow at Supercritical Reynolds Numbers. Jour. Aero./Space Sci., vol. 27, no. 11, Nov. 1960, pp. 801-13.

2. Schmidt, L. V.: Measurements of Fluctuating Air Loads on a Circular Cylinder. Calif. Inst. of Tech. Thesis, 1963.

3. Roshko, Anatol: Experiments on the Flow Past a Circular Cylinder at Very High Reynolds Number. Jour. Fluid Mech., vol. 10, pt. 3, May 1961, pp. 345-56.

4. Buell, Donald A., McCullough, George B., and Steinmetz, William J.: A Wind-Tunnel Investigation of Ground-Wind Loads on Axisymmetric Launch Vehicles. NASA TN D-1893, 1963.

FIGURE TITLES

Fig. 1.- Models.

Fig. 2.- Model A with conduits.

Fig. 3.- Model A with umbilical tower.

Fig. 4.- Bending moments on model A.

Fig. 5.- Lateral response coefficient for model A.

Fig. 6.- Response of model A with upstream conduit.

Fig. 7.- Response of model A with upstream conduit and plate under nose; conduit on upper stage.

Fig. 8.- Response of model A with two conduits.

Fig. 9.- Response of model A with 135° conduit.

Fig. 10.- Response of model A with upstream tower.

Fig. 11.- Model B - upper portion.

Fig. 12.- Response of model B.

Fig. 13.- Response of model C.

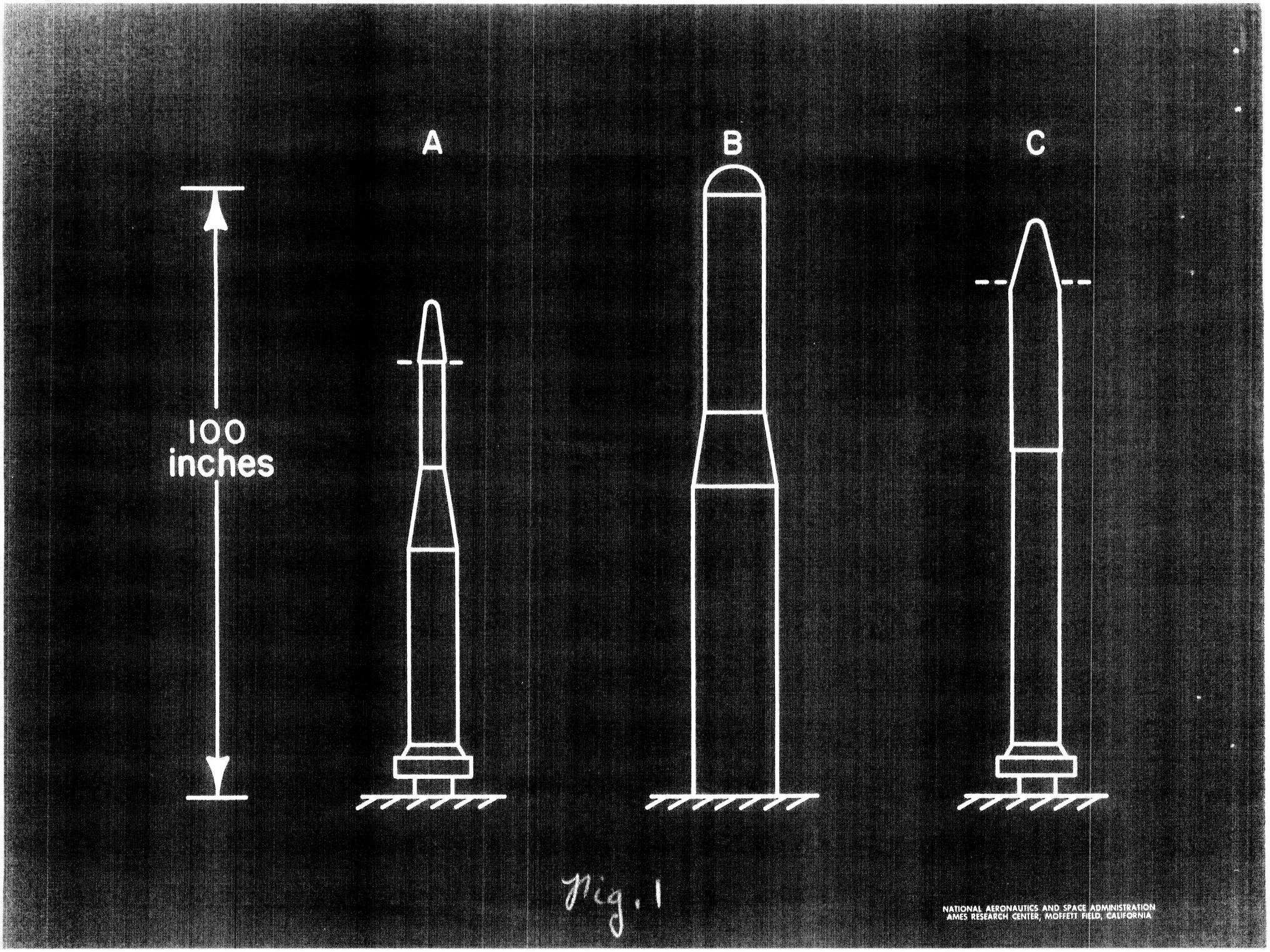

Fig. 1

NATIONAL AERONAUTICS AND SPACE ADMINISTRATION
AMES RESEARCH CENTER, MOFFETT FIELD, CALIFORNIA

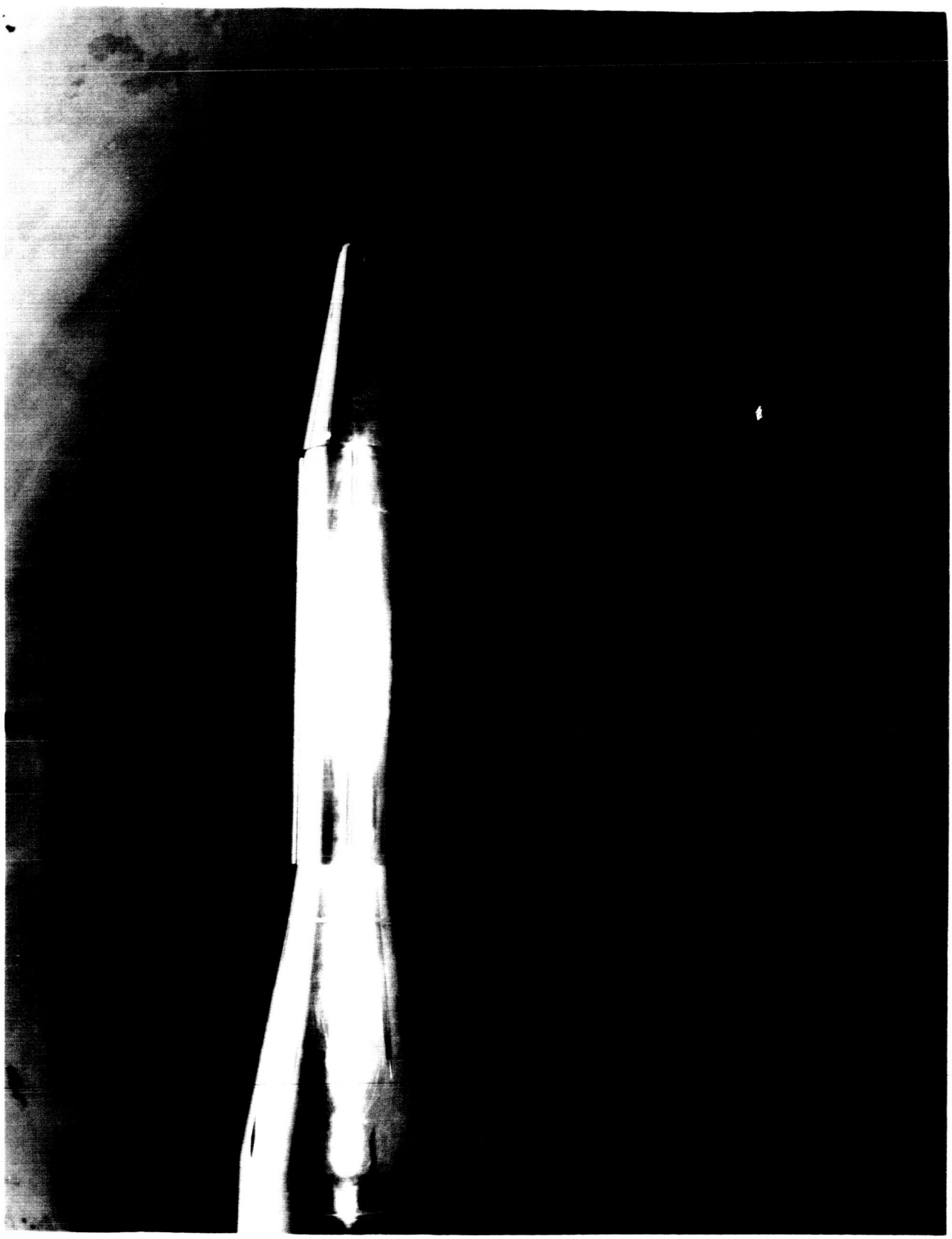

A-30563

Fig. 2. - Model A with conduits.

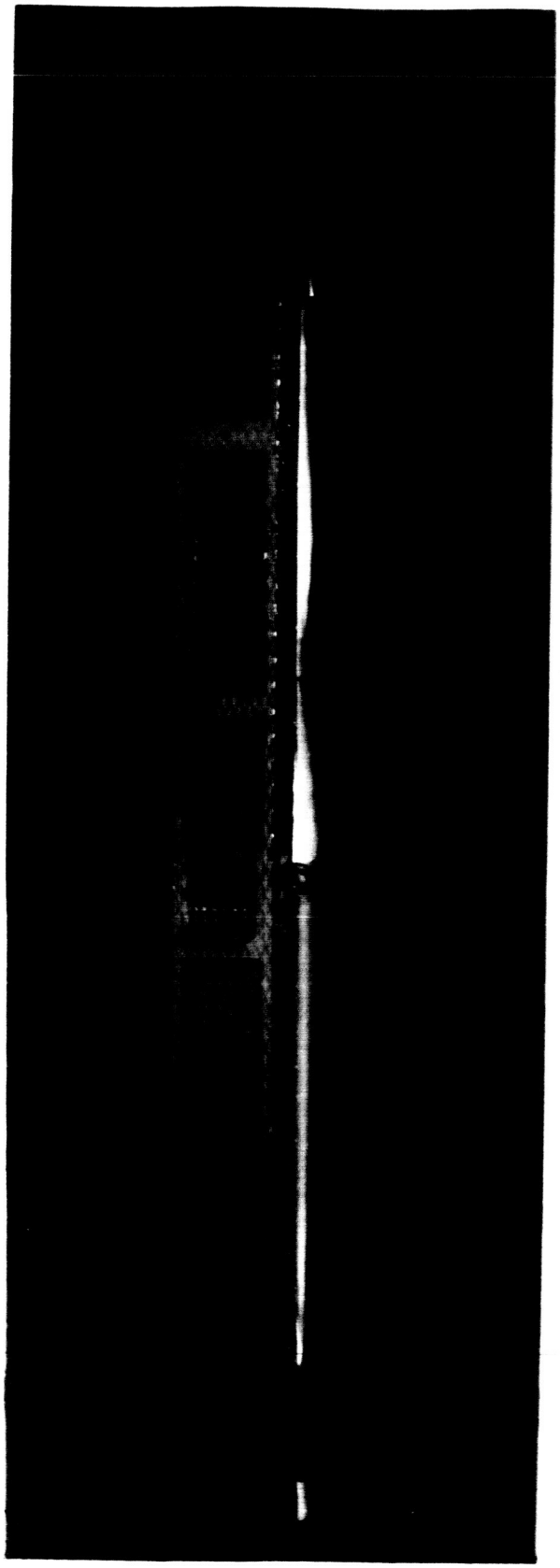

Fig. 3. - Model A with umbilical tower.

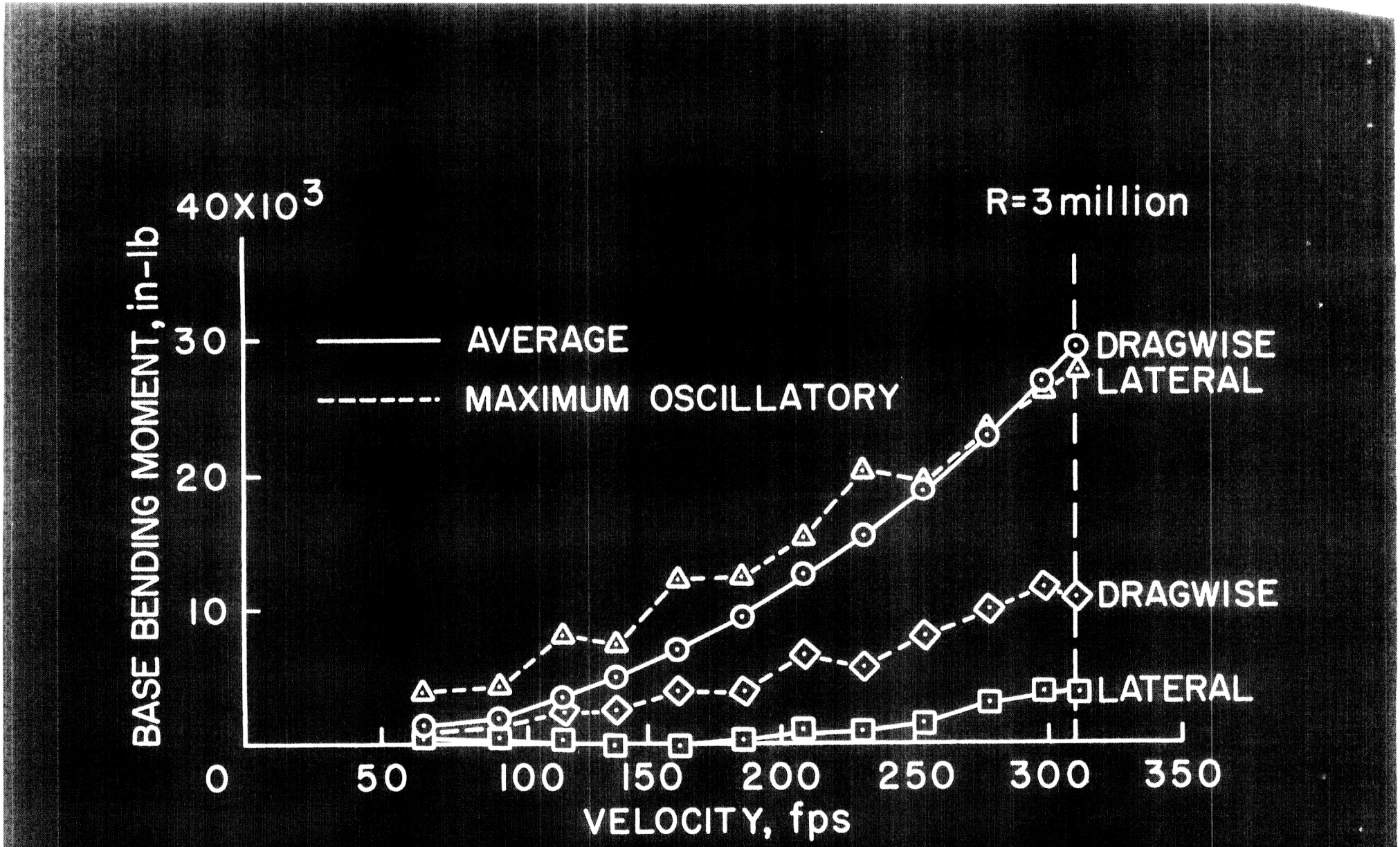

Fig. 4

NATIONAL AERONAUTICS AND SPACE ADMINISTRATION
AMES RESEARCH CENTER, MOFFETT FIELD, CALIFORNIA

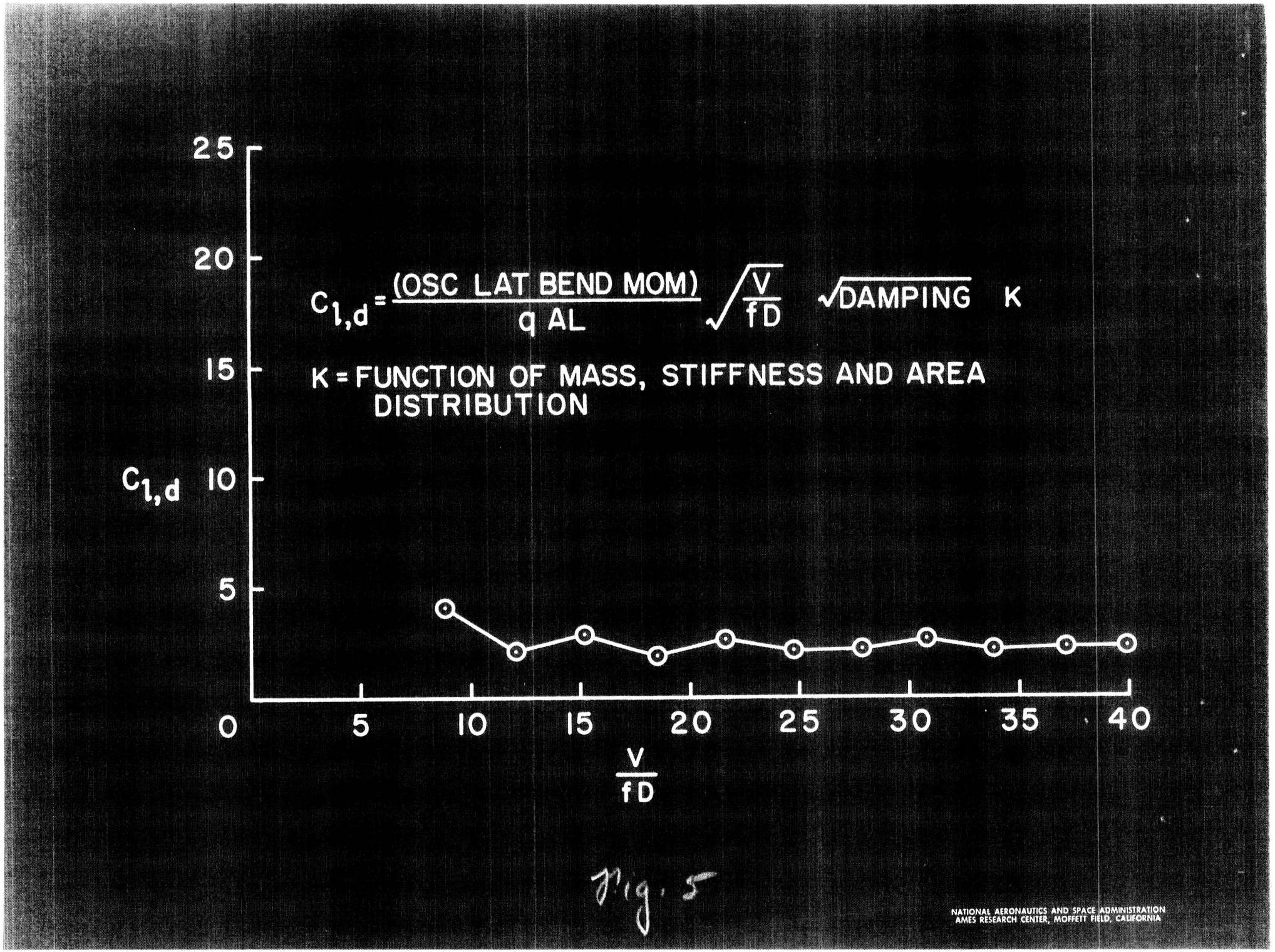

Fig. 5

NATIONAL AERONAUTICS AND SPACE ADMINISTRATION
AMES RESEARCH CENTER, MOFFETT FIELD, CALIFORNIA

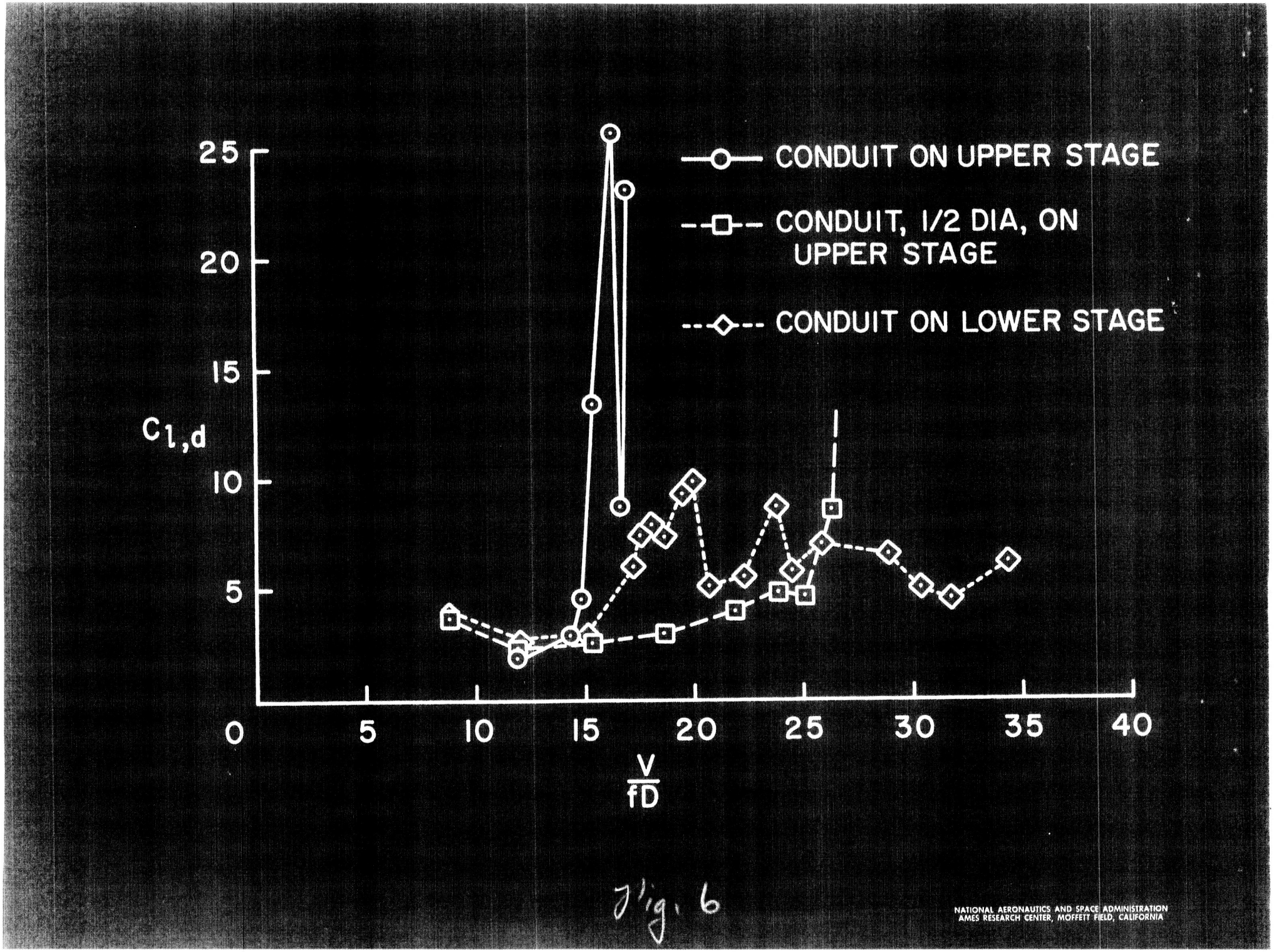

Fig. 6

NATIONAL AERONAUTICS AND SPACE ADMINISTRATION
AMES RESEARCH CENTER, MOFFETT FIELD, CALIFORNIA

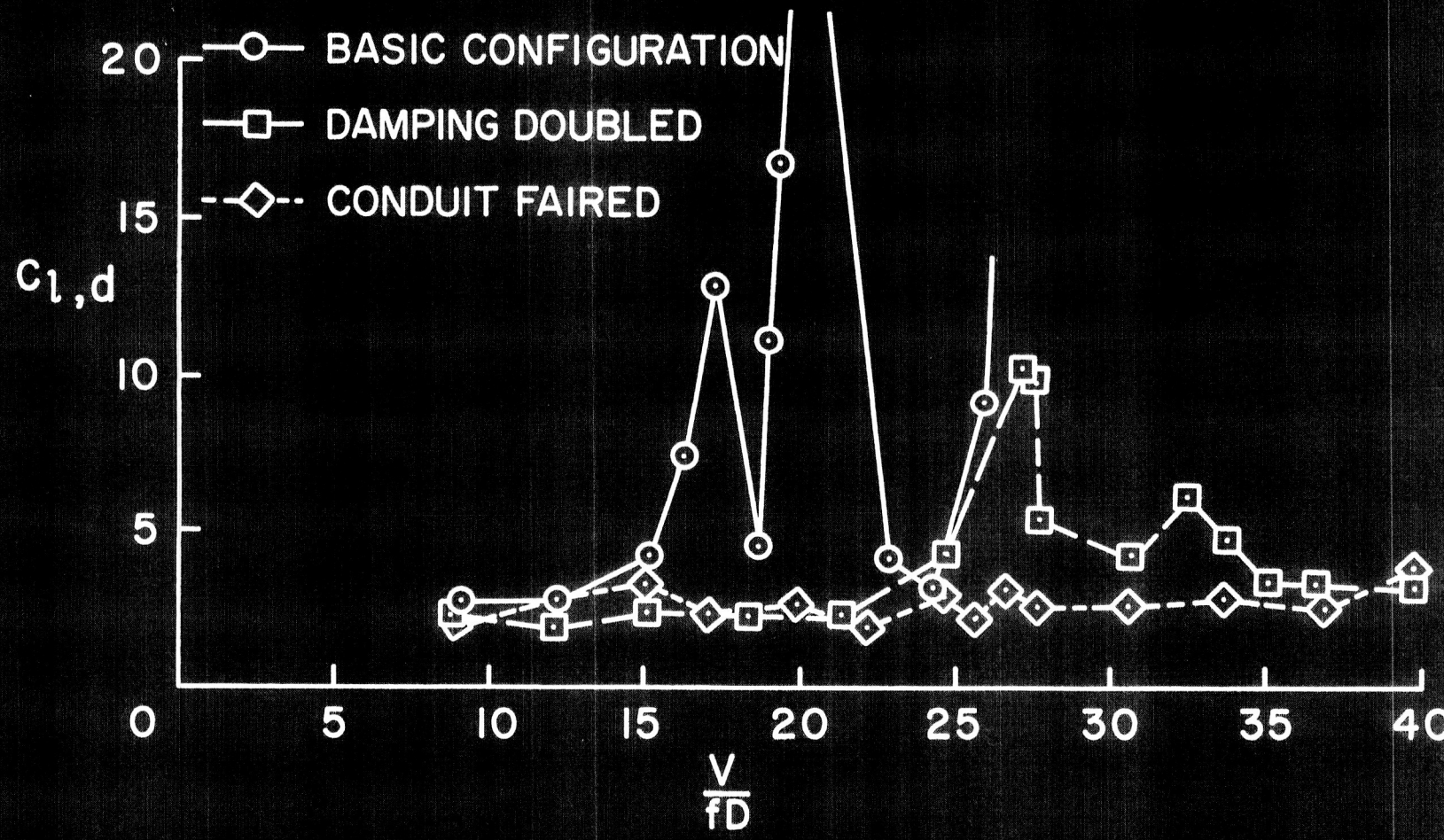

Fig. 7

NATIONAL AERONAUTICS AND SPACE ADMINISTRATION
AMES RESEARCH CENTER, MOFFETT FIELD, CALIFORNIA

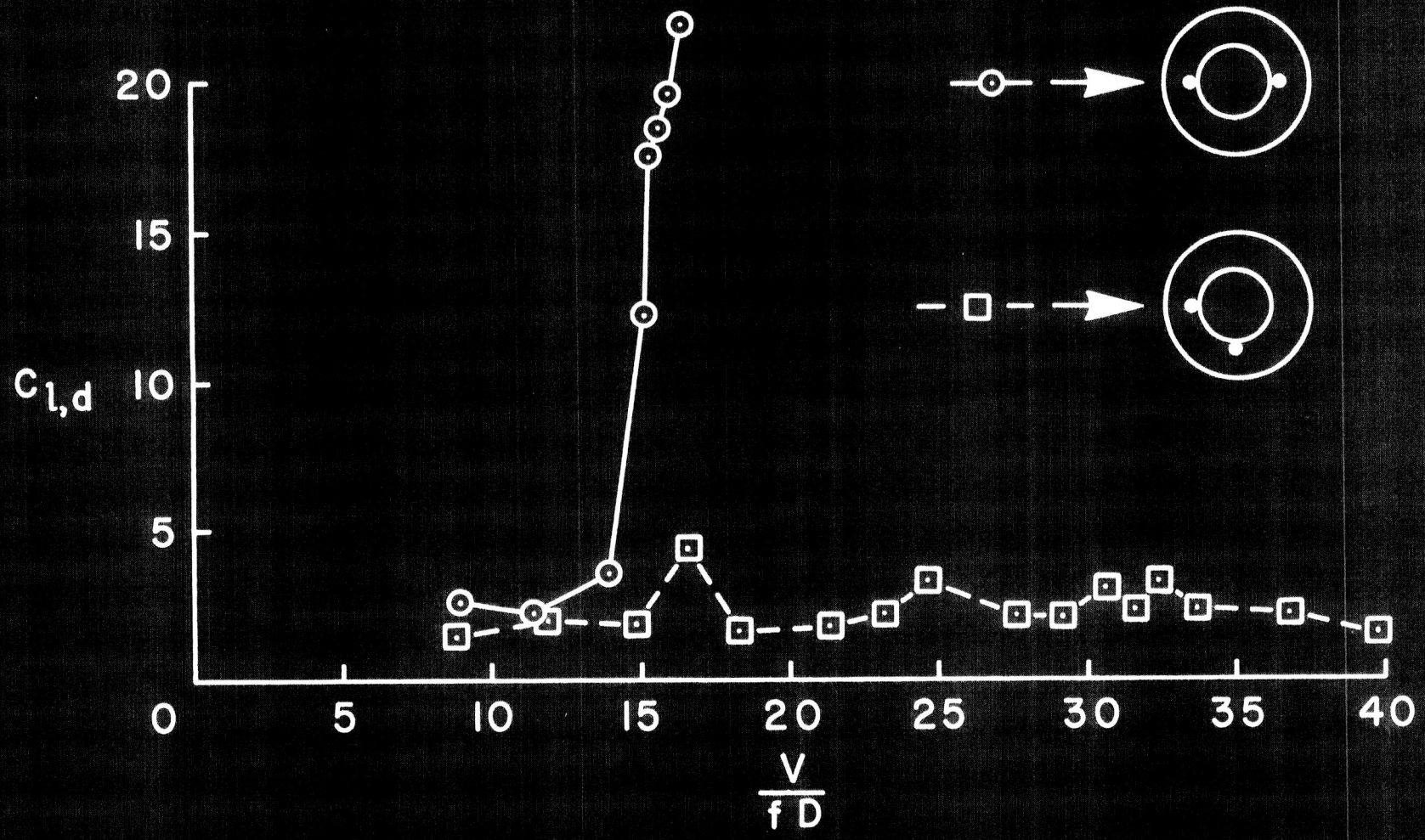

Fig. 8

NATIONAL AERONAUTICS AND SPACE ADMINISTRATION
AMES RESEARCH CENTER, MOFFETT FIELD, CALIFORNIA

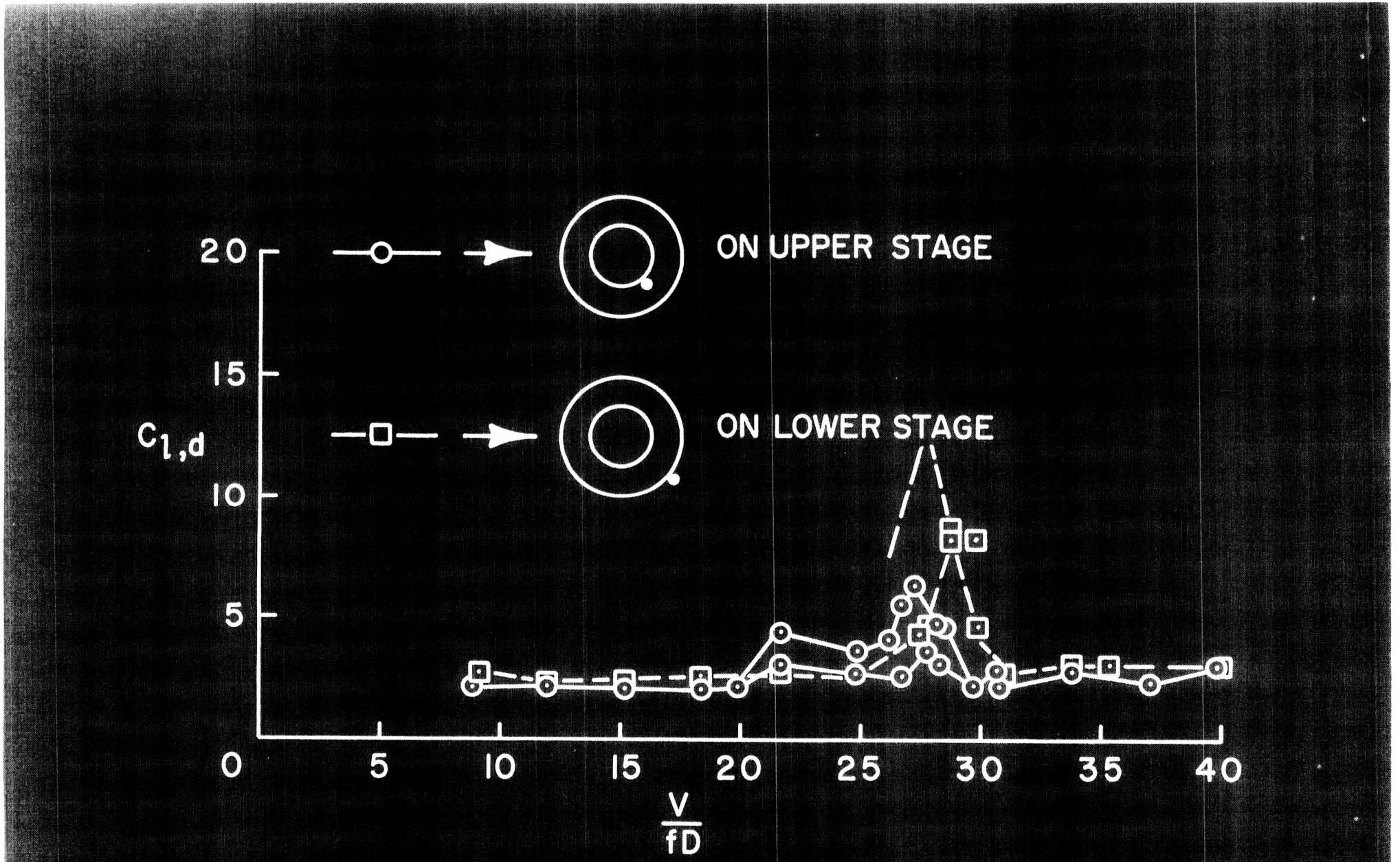

Fig. 9

NATIONAL AERONAUTICS AND SPACE ADMINISTRATION
AMES RESEARCH CENTER, MOFFETT FIELD, CALIFORNIA

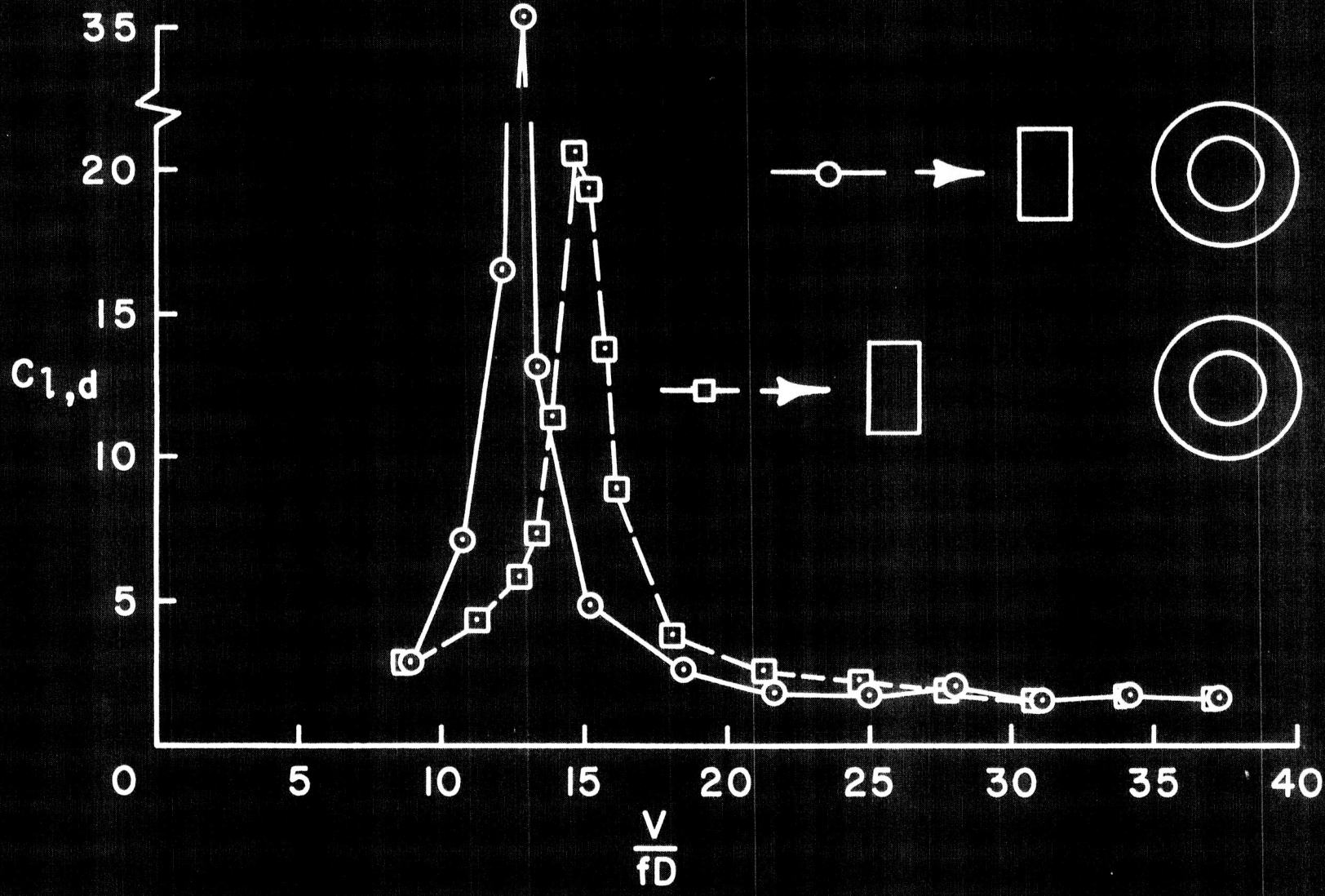

Fig. 10

NATIONAL AERONAUTICS AND SPACE ADMINISTRATION
AMES RESEARCH CENTER, MOFFETT FIELD, CALIFORNIA

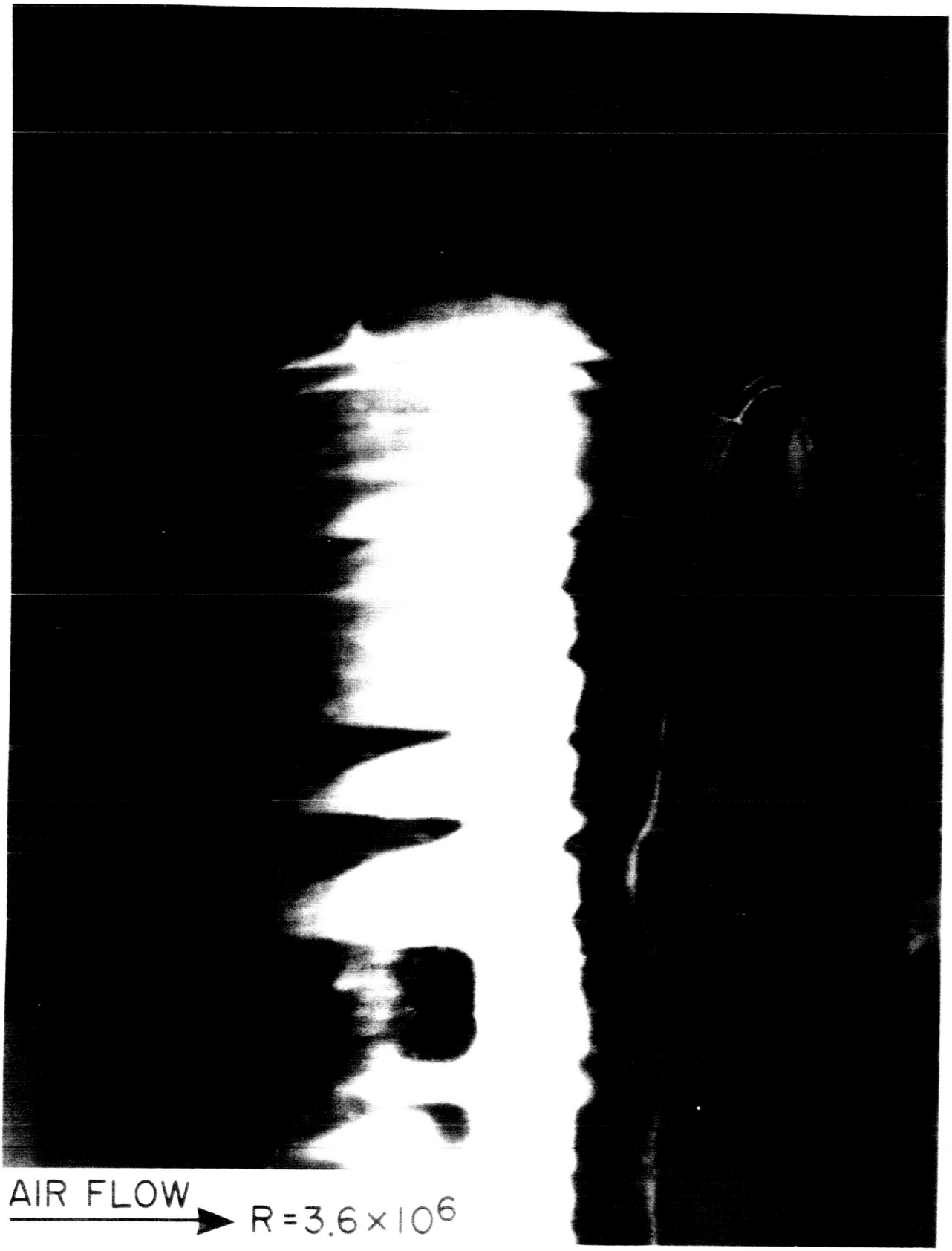
AIR FLOW
R = 3.6 × 10^6

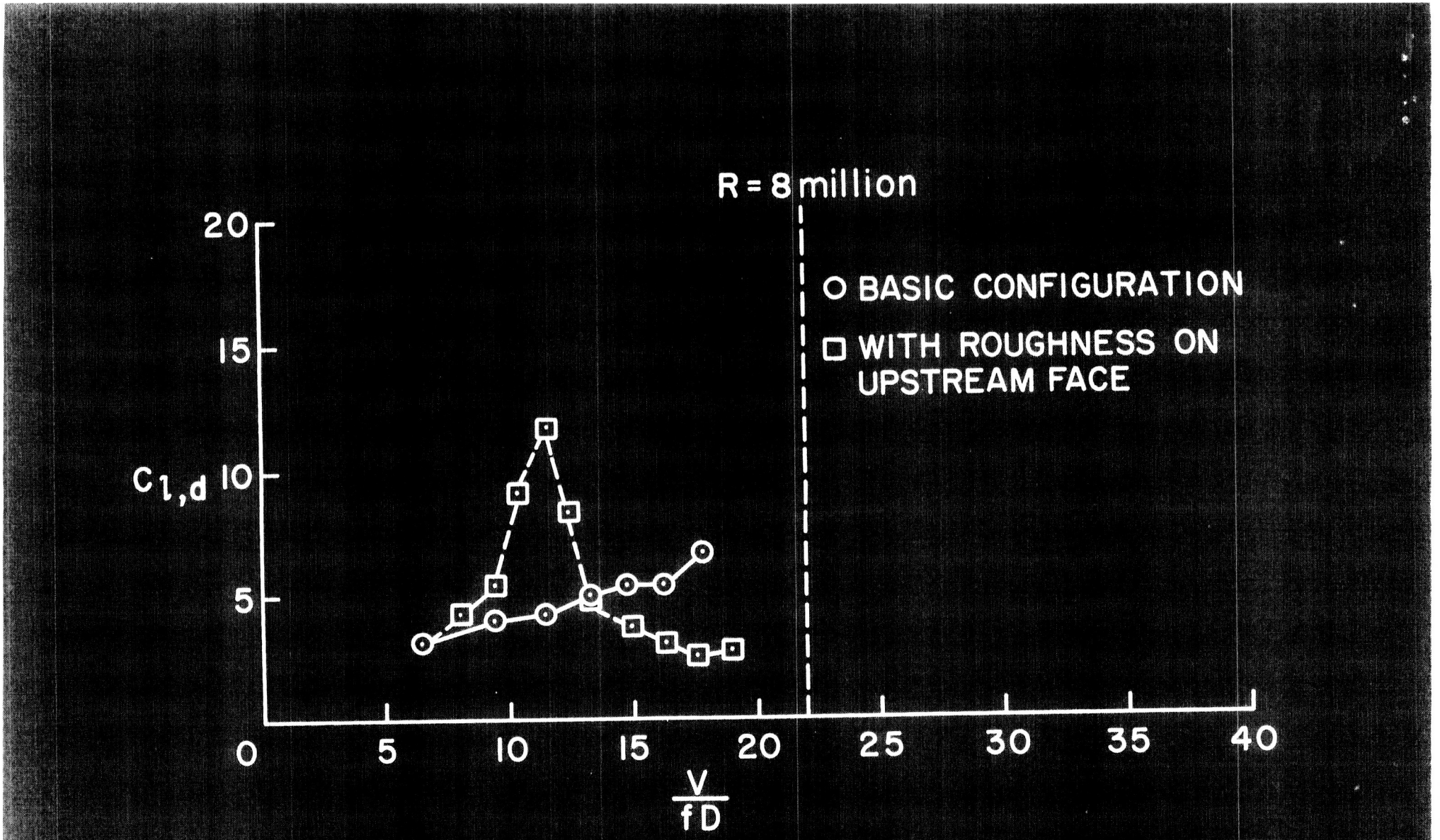

Figure 12

NATIONAL AERONAUTICS AND SPACE ADMINISTRATION
AMES RESEARCH CENTER, MOFFETT FIELD, CALIFORNIA

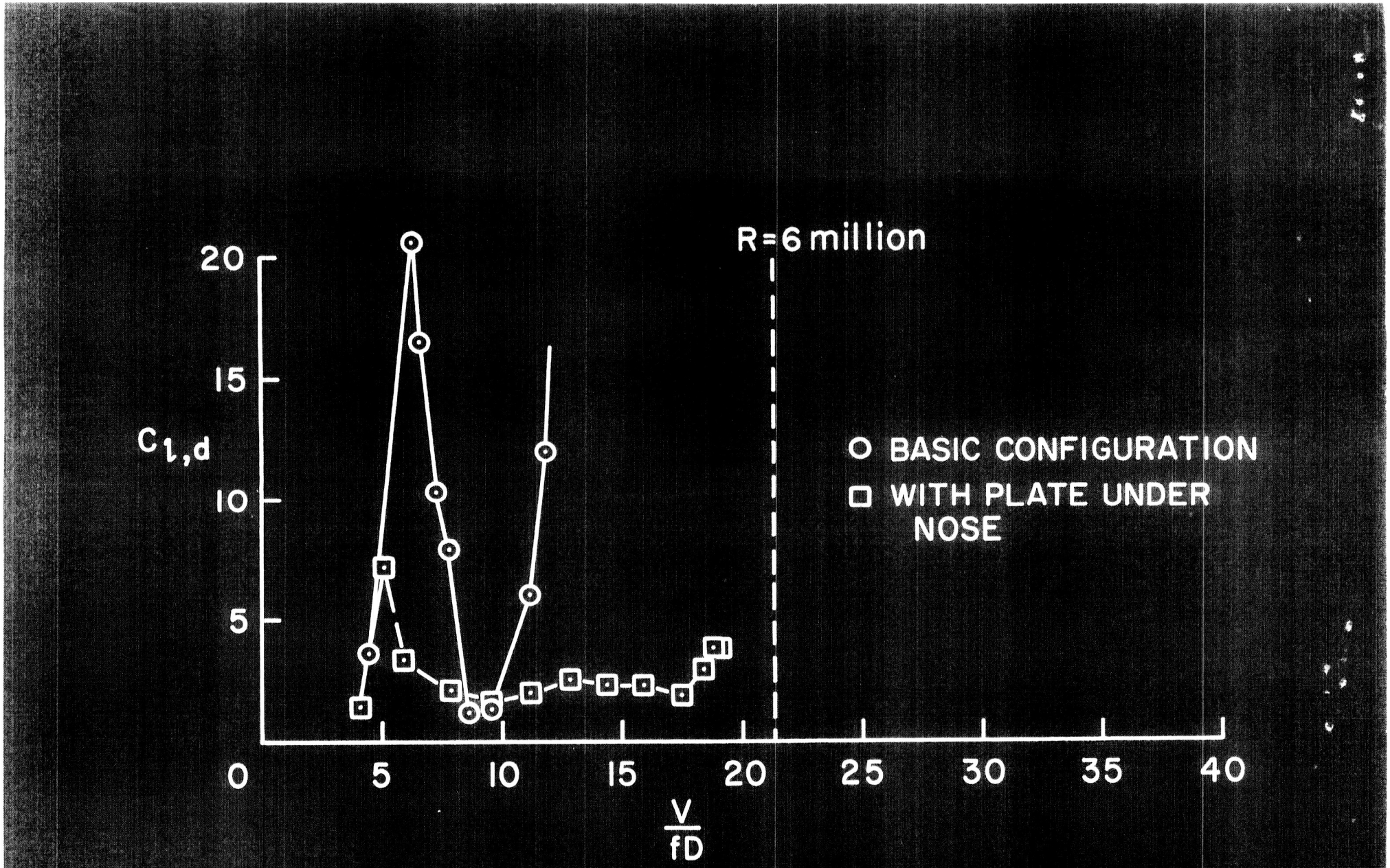

Fig. 13

NATIONAL AERONAUTICS AND SPACE ADMINISTRATION
AMES RESEARCH CENTER, MOFFETT FIELD, CALIFORNIA